5-11-2002

Detection of Knots in the Logs Using Finite Element Analysis

Satya Prakash Bikkina

DETECTION OF KNOTS IN THE LOGS USING FINITE ELEMENT ANALYSIS

By

Satya Prakash Bikkina

A Thesis
Submitted to the Faculty of
Mississippi State University
in Partial Fulfillment of the Requirements
for the Degree of Master of Science
in Electrical Engineering
in the Department of Electrical and Computer Engineering

Mississippi State, Mississippi

May 2002

DETECTION OF KNOTS IN THE LOGS USING FINITE ELEMENT ANALYSIS

By

Satya Prakash Bikkina

Approved:

Philip H. Steele Professor of Forest Products (Director of Thesis)	Nicholas H. Younan Professor of Electrical and Computer Engineering (Graduate Coordinator and Major Advisor)
Marion Hagler Professor of Electrical and Computer Engineering (Committee Member)	Wayne Bennett Dean of the College of Engineering

Name: Satya Prakash Bikkina

Date of Degree: May 11, 2002

Institution: Mississippi State University

Major Field: Electrical Engineering

Major Professor: Dr. Nicholas H. Younan

Title of Study: DETECTION OF KNOTS IN THE LOGS USING FINITE ELEMENT ANALYSIS

Pages in Study: 51

Candidate for Degree of Master of Science

The detection of internal log defects has been shown to have a potential for increasing the lumber value. As an alternative to other available expensive log scanning devices, a method using radio frequency waves has been used to detect the knots. The main focus of the current research is to investigate the effectiveness of using radio frequency waves to detect the knots. Electrostatic finite element analysis is performed to predict the defects in logs. A script has been written using the commercial finite element ANSYS software to predict defects in log sections. The results are then compared with the experimental data measured on actual log sections. Analysis proved that it is possible to detect presence of knots in the log sections.

ACKNOWLEDGMENTS

I would like to primarily thank Dr. Philip Steele, my research advisor, for his guidance, continuing assistance and financial support throughout this work. I want to thank my committee members for their valuable comments and suggestion. I would like in particular to acknowledge Dr. Nicholas Younan, who has significantly contributed to my learning experience during my graduate and research studies and the support he has given both financially and academically. I would like to thank Mr. Jerome Cooper for his help in performing the Statistical Analysis and for useful discussions pertaining to the theoretical aspects of my research. I would also like to thank Mr. Brian Mitchell for his help in data collection.

TABLE OF CONTENTS

LIST OF TABLES

LIST OF FIGURES

CHAPTER I

INTRODUCTION

1.1 Overview

Researchers have shown that the lumber value may be increased during sawing by the knowledge of internal log defect location followed by orientation of the log on the carriage [1,2]. Differential orientation of the log can change the position of defects contained in the sawn lumber and can significantly improve the lumber value. Tsolakides used computer simulation to test the influence of four rotational log positions and three sawing methods on the lumber value yield [1]. Red oak logs were selected from each of the three U.S. Forest Service standard log grades. He obtained an average increase of 21% in the lumber value when the highest value log orientation was compared to that at the lowest value.

Richards et al. used a mathematical algorithm to generate red oak knots in 63 computer generated conical logs [3]. These logs were sawn by computer simulation at 12 rotational positions. The simulations yielded an increase of 11% in the lumber value comparing the best log orientation to the worst. Peter obtained internal defect data with a larger sample of logs [4]. He manually simulated the sawing by manipulating the transparent overlays. From this simulated live sawing of 50 yellow poplar logs, he found a 9% increase in the lumber value.

Wagner et al. used 10 southern pine logs to determine the effect of sawing pattern and circumferential log orientation on the value of lumber sawn on a chipping headrig [2]. They found that each log had an optimum position that produced lumber of the highest value. Though clear logs showed little variation in value due to the log orientation, knotty logs showed a variation of about 43% in value.

Steele et al. used 24 red oak sawlogs; eight from each of the three hardwood log grades for obtaining internal defect data [5]. Simulations on both the live and grade sawing were performed. From the simulations, they found a 10% increase in the lumber value for both the live and grade sawing when logs were sawn at the highest value compared to average value yielding orientation.

These yield increases based on the simulations performed show a significant potential for the application of internal log scanning technology.

1.2 Potential Log Scanning Devices

Log internal defect detection technology has been based on a scanning device that collects a large amount of tomographic images that reveals the inner structure of the log. Today there are a variety of scanning technologies originating from medical applications such as X-Ray Computer Tomography (CT) scanning, X-Ray tomosynthesis, NMR scanning, microwave scanning and ultrasonic scanning. Since commercialization of scanners for medical diagnostic purposes is a relatively new phenomenon none of the scanning technologies identified are commercialized for the wood products industry.

Among the known potential methods of log scanning for internal defects, CT imaging is the most common solution for obtaining images because of its simplicity and

straightforward method of imaging [6-8]. There are two X-Ray based scanning approaches based on the method of rotation to obtain images [9]: the log rotation method and the X-ray source rotation method [10]. In the log rotation method, images of the log are taken by rotating the log between fixed radiation source and detector. However, this method is not practical for industrial purpose as it is difficult to rotate full-length logs [11]. An improvement to the log rotation method is using fixed radiating sources, which consists of several X-ray devices that obtain images from different angles [12]. Some of the advantages of this type of system are the absence of moving parts and high production rates [13]. The disadvantage is that very limited number of projections is obtained which produces a very coarse model of the interior of the log.

Brian et al. used a Siemens Somatom DR2 scanner for obtaining images of both green and dry wood samples of cedar, hemlock and fir [14]. Sindre et al. used green logs of Norwegian spruce for detecting internal log defects [15]. Both the groups were successful in obtaining the cross sectional pictures of the wood structure. However the speeds at which these images were produced were very slow and are not applicable for industrial purposes.

Recently, much CT imaging research for log scanning is based on developing efficient image analysis technologies to improve the operation speed [6]. Schmoldt et al. proposed a neural net-based classification technique for improving the accuracy and speed of internal log defect detection [16]. This image interpretation system increased scan rate and had an accuracy of about 95%.

Chang et al. proposed a NMR imaging method for log scanning [17]. They conducted experiments using a Siemens 0.5 Tesla Magnetom whole-body scanner. Two

white oak logs, 15 and 25 cm diameter respectively, and one black cherry log of 25.5 cm diameter were scanned. Two different coils scanned the logs. The smaller head coil produced higher resolution images than the body coil. However, for the industrial purposes, the images produced by the body coil were considered of more than sufficient resolution.

Schafer disclosed an apparatus based on the application of ultrasonic waves to detect localized anomalies such as knots and voids [18]. The apparatus applied one or more pairs of opposed ultrasonic transducers positioned perpendicular to the grain of the wooden member. A transmitting transducer generated an ultrasonic signal that passed through the log. A receiving transducer received the signal on the opposite side of the log. The detected ultrasonic beam was compared to a standard to detect a distortion in the waveform caused by the variation in the wooden member within the region. A commercial device based on this patent began to be used in 2000 for scanning cants [18]. The mechanism of scanning logs with ultrasound has not been solved and no commercial device is currently available.

1.3 Detection of localized anomalies by Microwaves and Radio frequency waves

Microwaves and radio frequency waves have been applied to detect anomalies in lumber and other panel materials. Anomalies interact with the electromagnetic radiation passing through the material. These methods are based on the fact that changes occur in the radiation passing through the lumber and the radiation reflected when a knot occurs in the applied field.

U.S. Patent No. 3,549,986 issued to Prine describes a system for detecting flaws in a wood sample [19]. The detection is based on the measurement of scattered energy by the flaws in the sample. This system is primarily intended to find inhomogeneties rather than the detection of knots or grain direction. U.S Patent No. 4,123,702 to Kinanen et al., and U.S. Patent No. 4,500,835 to Heikkila are related to the detection of knots and grain angle respectively in lumber using microwaves [20,21]. These systems employ a detection means that is sensitive to the energy transmitted directly from a transmitting antenna and the energy reflected from the surfaces of the material. All the methods that are described above are costly to implement since they use microwaves, which are high frequency radio waves and require wave-guides for generation and detection.

U.S. Patent No. 4,972,154 issued to Bechtel disclosed a device capable of measuring wood grain angle and also for detecting knots and voids on a cut surface such as lumber or veneer [22]. This device determines the grain angle based on the differences in the dielectric response with the application of radio frequency signal to one surface of the wood and measuring the response at different angles. The wood slope of the grain is determined by the sampling of the electrical field by a sensor with receiving electrodes arranged in a circular configuration around a sending electrode. The electric field is sampled at 8 different angles. Grain direction is determined based on the angle from which the highest dielectric response value is received.

Steele and Kumar in U.S. Patent No. 5,585,732 disclosed a device for determining the location of knots and voids in wood and for estimating wood strength [23]. The device uses multiple capacitors for signal generation and receiving. The computer automatically displays the void and knots. The calibration function is also done

automatically. None of the radio frequency devices disclosed have been used to detect anomalies in logs, trees or poles.

The closest prior art to the device disclosed here is a microwaveable device described by Kaestner, who disclosed an internal log defect detection system based on application of microwaves [9]. In this system, the scanning is performed using Frequency Modulated Continuous Wave (FM-CW) Radar which is linearly polarized into two waves, one parallel to direction of fibers and the other in the direction perpendicular to the fibers, in the frequency band 2-18 GHz using seven overlapping 4 GHz subbands and by rotating the log by 360^0 in steps of 1^0.

Kaestner's experiments were mainly concentrated for the three frequency bands 2-6 GHz, 4-8 GHz and 8-12 GHz. Results showed that the images produced in the 4-8GHz range produced images of highest contrast. The images are produced using the data from stoke parameters, polarization ratio, and the state of polarization. This system however, is currently not suitable for industrial application as the log is mounted firmly and rotated instead of moving it axially. It also requires a transmitting and a receiving antenna and a high-energy source to generate the microwave signal.

A device similar to the Kaestner device was disclosed by Svenson et al [24]. This is a three dimensional microwave tomographic system that is capable of imaging biological objects by determining tissue dielectric property differences within the object. Multiple frequencies, which range from 100 kHz to 6 GHz, are transmitted through the tissue that is placed in-between a set of transmitters and receivers arranged in a ring. Analysis of the received radiation to obtain observed tissue dielectric values, and

comparing them with the expected values allows imaging of the structures. Again, wave guides are required to transmit and receive the microwave signals.

One of the main applications of radio frequency waves is in the field of Electrical Capacitance Tomography. U.S. Patent No. 5,130,661 to Beck et al. describes a two-component tomographic flow imaging system that is capable of monitoring the flow in a pipe [25]. The system uses eight capacitance electrodes positioned around a pipe through which a flow to be monitored passes. A predetermined voltage signal with a frequency of 2 MHz is applied to each of the electrodes at different instances of time, and then the capacitance between each pair of electrodes is measured. Based on the measured capacitance values an image representative of the distribution of material within the pipe is obtained by using an image reconstruction algorithm.

No previous devices are disclosed in patents or literature that employ electrodes to detect knots in green logs with radio frequency waves. The finite element analysis to simulate the electromagnetic response of logs and contained knots has not previously been performed.

The main focus of the current research is to investigate the effectiveness of using radio frequency waves to detect knots. Finite element ANSYS software is used to predict defects in the log sections. Chapter II discusses in brief the properties of wood. Chapter III focuses on the finite element theory. The experimental procedure used to gather voltage data on log sections is discussed in chapter IV. Chapter V deals with the simulation model construction developed in ANSYS software. In chapter VI, the analysis and results are discussed. Finally chapter VII provides a summary of the work done and the future work necessary to improve the model.

CHAPTER II

PROPERTIES OF WOOD

Dry wood is a good electrical insulator [29]. However, the presence of moisture increases the electrical conductivity considerably. According to electromagnetic theory, the relation between electric field intensity vectors $\vec{E}$, electric displacement vector $\vec{D}$ is given by $\vec{D} = \varepsilon * \vec{E}$, where ε is the dielectric permittivity of the medium or material i.e., $\varepsilon = \varepsilon_0 \varepsilon_r$ with ε_0 being permittivity of free space and ε_r being relative permittivity of dielectric material. In general, some of the properties of wood can be characterized by the dielectric constant, frequency of input signal, moisture, and density and conductivities. These parameters are described below.

2.1 Dielectric constant

When an electric field is applied to a parallel plate capacitor, the dielectric material between the two electrodes exhibits an ability to absorb and store electric potential energy in the form of polarization. This ability of the material is known as the dielectric constant. The energy stored in the dielectric is measured in terms of capacitance, which is defined as the ratio of charge on one electrode to the potential difference between the two electrodes. For example the capacitance between two parallel plate electrodes with air as the medium is given by

$$C = \varepsilon * A/d$$

where:

ε = dielectric constant of the medium or material,

A = area of electrode surface,

D = distance between the electrodes.

In terms of capacitance, the dielectric constant is defined as the ratio of the capacitance of a given capacitor with the material as the insulator to the capacitance of the same capacitor with air as the insulator [28].

2.2 Frequency

When an alternating current (AC) signal is applied to a dielectric material, the polarization of the electric field, the rate of variation with time of the external electric field is periodically reversed. This rate of variation is determined by the frequency of the alternating signal. As the applied signal frequency increases, the rate of polarization also increases, resulting in a decrease in the amount of energy stored in the dielectric. At high frequencies, the measurements become more sensitive to moisture and the signal will be attenuated to a degree that the detection of the received signal becomes almost impossible [30,31].

Experiments by Wittkopf and James reveal that the dielectric constant of wood decreases and loss tangent increases with an increase in frequency [30,32,33]. The large magnitude of polarization at low frequencies is due to the interfacial polarization, which is the polarization at discontinuities of the conductivity [34]. As the frequency increases, the molecular polarization (the energy is absorbed in the form of induced dipole

movement of the molecule and in the form of alignment of molecules) dominates the interfacial polarization. However, care must be taken while conducting the experiments. The maximum frequency that can be used is limited by the physical size of the electrode. If the frequency exceeds a certain limit, non-uniform heating of the electrodes may result. This effect is more prominent while using parallel plate capacitors. The wavelength, which is defined as the distance traveled by the signal, is expressed in terms of the frequency and dielectric constant given by [32]

$$\text{Wavelength} = \frac{984}{f * \sqrt{\varepsilon}} \text{ measured in feet (ft)}$$

Where:

f = frequency of the input signal,

ε = permittivity.

The maximum electrode dimension should not exceed more than approximately one-eighth of the wavelength.

2.3 Moisture

Wood is mainly composed of chemical constituents – cellulose, hemi-cellulose and lignin [35]. Among these components, cellulose is the most important molecule that gives mechanical strength since it resides in the cell walls. The structure of this molecule is shown in Figure 2.1.

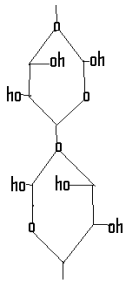

Figure 2.1: Illustration of the chemical structure of cellulose molecules.

The dielectric constant of wood increases with moisture content [35,5,36]. This increase in dielectric constant occurs because the dielectric constant of water is higher than that of cellulose. As the moisture content is increased, the rotation of polar groups in the cell wall and cellulose molecules also increases. Experiments have shown that the dielectric constant increases exponentially with moisture content below the fiber-saturation point, and then linearly above this point [34,36].

Wood with moisture content near the fiber saturation point displays an electrical resistivity of the order of 10^4 or 10^5 ohm-cm and at higher temperatures it is as low as 10^3 ohm-cm [37]. On the other hand, oven-dry wood has a resistivity of 10^{17}. Both the dielectric constant and loss tangent exhibit discontinuities at 6 percent moisture content [36,37]. The effect of moisture on loss tangent shows a variation depending upon the temperature and frequency. The loss tangent increases as the moisture content is increased [37]. At frequencies higher than 1 MHz, this relationship no longer holds. The loss tangent in this case attains a maximum followed by a minimum.

2.4 Density and Conductivity

The conductivity of a material determines the amount of current that will flow when a potential is applied to the material. The conductivity can be expressed as [38]:

$$K = N * u * a * e$$

where:

N = total number of charge carriers per unit volume,

u = ionic mobility,

a = degree of dissociation,

e = ionic charge.

The product $N * a$ determines the concentration of conducting ions in wood. The main factors that affect the conductivity are the ionic mobility and degree of dissociation. Hearle concluded that the latter effect is most important in limiting the conductivity [5]. The degree of dissociation is mainly due to the fact that the water molecule, which is polar, weakens the strong interionic bond that exists in solids. Stamm noted that, for a given moisture content, wood that has twice the specific gravity should have double the conductivity of the lower specific gravity wood [39]. Experiments conducted by Venkateswaran confirmed these results. Wittkoff's experiment showed that as the density of wood increases, the dielectric constant and loss tangent also increase [38].

CHAPTER III

FINITE ELEMENT METHOD

3.1 Theoretical Background

The finite Element Method (FEM) is a mathematical technique for obtaining approximate numerical solutions to equations that gives the response of physical systems subjected to external loads [26]. Any physical problem, which may be a 1-D, a 2-D or a 3-D problem, can be represented in the form of a governing equation. For example, 1-D problems of a physical phenomena such as mechanical, electrical, and fluid flow that are based on conservation or balance of some physical property that can be represented by a differential equation that takes on a general form by [27]

$$\frac{d}{dx}\left[\alpha(x)\frac{dU(x)}{dx}\right] = f(x) \tag{3.1}$$

The above equation is a combination of two separate equations: a balance equation and a constitutive equation. A *balance equation,* which is based on the conservation principle (i.e. loss of energy is equal to gain of energy), is given by:

$$\frac{d\tau(x)}{dx} = f(x) \tag{3.2}$$

where $\frac{d\tau(x)}{dx}$ represents the loss of energy caused by some physical quantity across the boundaries, and $f(x)$ represents a gain of energy to the system. On the other hand, a constitutive equation is given by:

$$\tau(x) = \left[\alpha(x)\frac{dU(x)}{dx}\right] \tag{3.3}$$

where $\alpha(x)$ is a physical or material property, $\tau(x)$ represents force, stress or flow and $U(x)$ represents some boundary condition. Note that a direct substitution of equation (3.3) into equation (3.2) yields equation (3.1). In case of a stress analysis, $f(x)$ represents the force per unit volume, $U(x)$ represents the displacement, and $\alpha(x)$ represents the material property such as Young's modulus. For electrostatic cases, $f(x)$, $U(x)$, and $\alpha(x)$ represent the charge density, potential, and permittivity respectively. Accordingly, any physical problem that satisfies equation (3.1) can be solved numerically provided that the exact properties and boundary conditions are specified.

The analysis of any problem using the finite element method generally involves four basic steps [28]: (1) dividing the domain of interest into a finite number of smaller regions called elements. (2) deriving element equations (i.e. approximate solution) generally into algebraic form, from a system of governing equations. (3) Assembling all element solutions into a larger set of algebraic equations called system equations. (4) Solving the system equations using numerical analysis techniques. These steps are described below in relation to electromagnetics, more specifically electrostatics for a 2-D problem.

Division into elements:

The domain of the problem is divided into smaller regions called elements. In case of a 2-D problem, some of the basic elements are a triangle and a quadrilateral. These elements touch each other without overlapping and gaps between them as shown in Figure 3.1. The vertices of the elements are called nodes. The process of dividing a domain into small regions is called meshing. Meshing is generally performed using computers with programs called preprocessors.

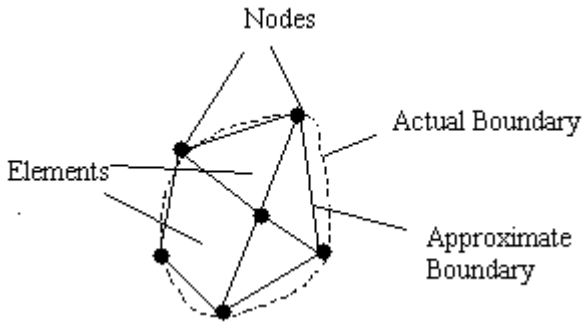

Figure 3.1: A typical finite element division of an irregular object

The approximate solution of potential for the whole region can be determined by knowing the potential of each element. That is

$$V(x,y) \cong \sum_{n=1}^{N} V_n(x,y) \tag{3.4}$$

where V_n is the potential of each element. If the element chosen is a triangle, then V_n can be approximated as

$$V_n(x,y) = a_1 + a_2 x + a_3 y \tag{3.5}$$

Deriving element equations:

Element equations that are an generally algebraic form of differential equations are identical for all elements of the same type. For example, in Figure 3.1 we have three triangular elements and one quadrilateral element. The three triangular elements have the same algebraic equation. Consider a typical triangular element as shown in Figure 3.2.

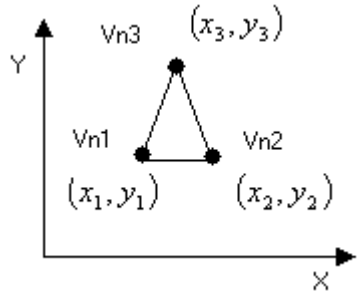

Figure 3.2: Typical triangular element

The potential at nodes 1, 2 and 3 are obtained by using equation (3.5), which can be written in matrix form as:

$$\begin{bmatrix} V_{n1} \\ V_{n2} \\ V_{n3} \end{bmatrix} = \begin{bmatrix} 1 & x_1 & y_1 \\ 1 & x_2 & y_2 \\ 1 & x_3 & y_3 \end{bmatrix} \begin{bmatrix} a_1 \\ a_2 \\ a_3 \end{bmatrix} \tag{3.6}$$

The coefficients a_1, a_2, a_3 can be obtained by taking the inverse of the above equation. Substituting the coefficients into equation (3.5) gives:

$$V_n = \begin{bmatrix} 1 & x & y \end{bmatrix} \frac{1}{2A} \begin{bmatrix} (x_2 y_3 - x_3 y_2) & (x_3 y_1 - x_1 y_3) & (x_1 y_2 - x_2 y_1) \\ (y_2 - y_3) & (y_3 - y_1) & (y_1 - y_2) \\ (x_3 - x_2) & (x_1 - x_3) & (x_2 - x_1) \end{bmatrix} \begin{bmatrix} V_{n1} \\ V_{n2} \\ V_{n3} \end{bmatrix} \tag{3.7a}$$

or

$$V_n = \sum_{i=1}^{3} \alpha_i(x,y) V_{ni} \tag{3.7b}$$

where A is the area of the element n, and $\alpha_i(x,y)$ the *element shape functions*.

The energy per unit length for element e is given by

$$W_n = \frac{1}{2}\int \varepsilon |E|^2 \, dS \tag{3.8}$$

For a two-dimensional solution region that is free of charge, $E = \nabla V_n$. Therefore equation (3.8) becomes:

$$W_n = \frac{1}{2}\int \varepsilon |\nabla V_n|^2 \, dS \tag{3.9}$$

But from equation (3.7b): $\nabla V_n = \sum_{i=1}^{3} V_{ni} \nabla_{\alpha i}$

Substituting the above equation into equation (3.9) gives:

$$W_n = \frac{1}{2}\sum_{i=1}^{3}\sum_{j=1}^{3} V_{ni} \varepsilon \left[\int \nabla_{\alpha i} \bullet \nabla_{\alpha j} dS\right] \bullet V_{nj} \tag{3.10}$$

The above equation can be written as:

$$W_n = \frac{1}{2}\varepsilon [V_n]^T \left[C^{(n)}\right][V_n]$$

where V_n are nodal potentials of the triangular element. And $\left[C^{(n)}\right]$, which is 3×3 matrix is called the *element coefficient matrix* and is given by

$$C_{ij}^{(n)} = \int \nabla_{\alpha i} \bullet \nabla_{\alpha j} dS$$

<u>*Assembling all elements:*</u> After deriving the corresponding equations for a typical element, the next step is to combine all such elements in the domain and obtain a system of equations. The energy associated with assembling all elements is given by

$$W = \sum_{n=1}^{N} W_n = \frac{1}{2}\varepsilon [V]^T [C][V] \qquad (3.10a)$$

where $[V] = [V_1 V_2 ... V_m]^T$, m is the number of nodes, N is the number of elements, and $[C]$ is called the *global coefficient matrix,* whose terms are equal to the sum of the individual element coefficient matrices.

Solving the system equations:

The final step in the analysis is to solve the system of equations to obtain the nodal potentials. It is known that Laplace's equation is satisfied when the total energy in the solution region is a minimum. To satisfy this, the partial derivative of W with respect to each nodal potential value is set to zero. That is

$$\frac{\partial W}{\partial V_1} = \frac{\partial W}{\partial V_2} = ... \frac{\partial W}{\partial V_m} = 0$$

or

$$\frac{\partial W}{\partial V_k} = 0 ; \quad k = 0,1,2,.....m.$$

In general, the above condition leads to $\sum_{i=1}^{m} V_i C_{ik} = 0$ using equation (3.10a).

The above equation is a system of simultaneous equations, which can be solved by iterative methods to obtain nodal potentials. From the nodal potentials, element potentials and finally the domain potentials can be obtained as shown by the equations derived above.

3.2 Expansion to a 3-D case

The finite element theory discussed in the previous section can be extended to 3-D elements. As discussed, the first step is to divide the domain into smaller regions called elements. In case of a 3-D problem, the basic elements are a tetrahedron or a hexahedron. The approximate solution of potential for the whole region can be determined by knowing the potential of each element. That is

$$V(x,y,z) \cong \sum_{n=1}^{N} V_n(x,y,z) \tag{3.11}$$

For a tetrahedron, V_n can be approximated as

$$V_n(x,y,z) = a_1 + a_2 x + a_3 y + a_4 z \tag{3.12}$$

After element discretization, element equations can be derived as follows. The potential at nodes can written in matrix form as:

$$\begin{bmatrix} V_{n1} \\ V_{n2} \\ V_{n3} \\ V_{n4} \end{bmatrix} = \begin{bmatrix} 1 & x_1 & y_1 & z_1 \\ 1 & x_2 & y_2 & z_2 \\ 1 & x_3 & y_3 & z_3 \\ 1 & x_4 & y_4 & z_4 \end{bmatrix} \begin{bmatrix} a_1 \\ a_2 \\ a_3 \\ a_4 \end{bmatrix} \tag{3.13}$$

The coefficients a_1, a_2, a_3, a_4 can be solved by taking the inverse of the above equation. The values of the coefficients can then be substituted in equation (3.12) and an equation similar to equation (3.7b) can derived as

$$V_n = \sum_{i=1}^{4} \alpha_i(x,y,z) V_{ni} \tag{3.14}$$

where $\alpha_i(x,y,z)$, the *element shape function,* is given by:

$\alpha_i(x,y,z) = \frac{1}{6v}\left(a_i + a_i x + a_i y + a_i z\right)$, with v being the volume of the element.

The energy per unit length for element *e* can be derived using the same procedure described in the previous section. However, the element coefficient matrix in case of a 3-D element is written as $C_{ij}^{(n)} = \int \nabla_{\alpha i} \bullet \nabla_{\alpha j} dv$. After deriving the element equations, the nodal potentials and the domain potentials can be obtained using the same procedure described for a 2-D problem.

3.3 Relationship to wood properties

The domain potential, which is the boundary or output potential, is highly influenced by the properties of a given material. For wood the primary influences are the density, moisture content and permittivity of the wood, and the frequency of the applied signal. As the permittivity of wood increases, the output potential is expected to increase since the ability to conduct electricity increases. As discussed in Chapter II, the dielectric constant of wood increases as the moisture content and density of the material increase, while dielectric constant decreases as the frequency of the signal increases. Hence the domain potential increases with an increase in moisture content and density, while it decreases with increase in frequency of the signal.

CHAPTER IV

EXPERIMENTAL PROCEDURE

4.1 Objective

The objective of this study is to detect the presence of knots in green logs with radio frequency signals passed through the log diameter and to simulate the expected results with the finite element method.

4.2 Hardware arrangement

The block diagram of the system for obtaining the voltage readings is shown in Figure 4.1. The voltage sensing apparatus consisted of six evenly spaced electrodes attached to an elastic band that will be termed the *electrode collar*. A Wavetek .2-2200 MHz synthesized signal generator and radio frequency (RF) power amplifier generated a high-power radio frequency signal. The signal from the amplifier was applied to the electrodes by manually switching among electrodes attached to the log section. The output peak-to-peak voltage values from the receiving electrodes were measured using an oscilloscope.

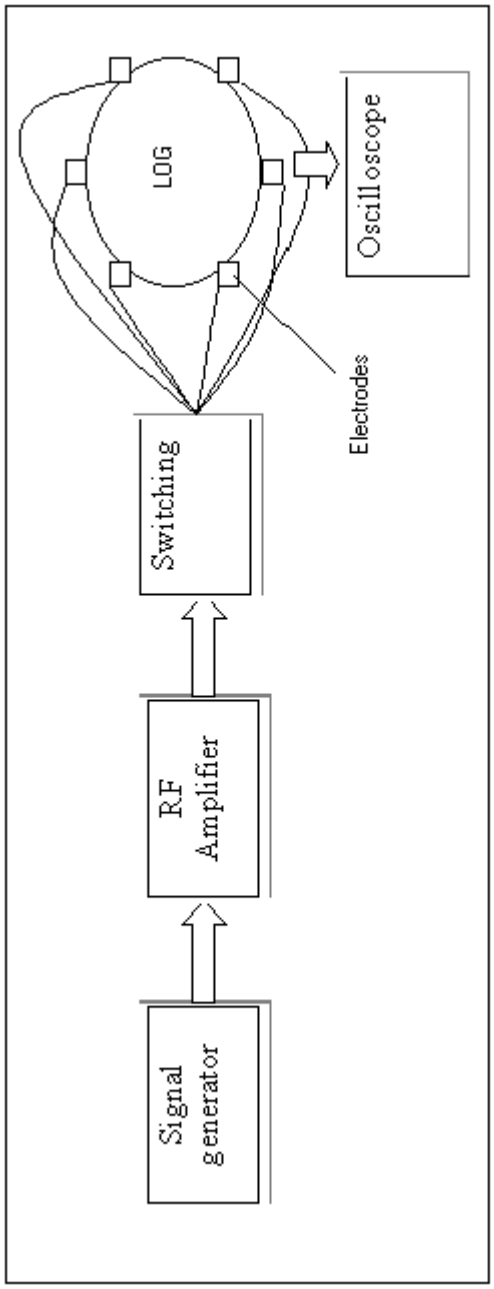

Figure 4.1 Block diagram of the system used to obtain voltage readings.

4.3 Experimental Procedure

Three trees were selected that were 10,11, and 12 inches in diameter respectively, at diameter breast height. The trees were felled and three 3-foot sections from each tree were cut beginning at 2-feet from the ground level. Log sections were carefully marked to indicate within-tree orientation. Logs were placed in cold storage at 32^{o} F.

Just prior to gathering data from the electrodes, each log section to be scanned was thawed, debarked with a draw knife, and planed with a hand-held electric planer to remove surface irregularities as well as taper. Removal of irregularities and taper kept the distance between electrodes identical and removed the need for data correction due to variance in distance between electrodes. Six lines, equidistant around log circumference were inscribed down log-section length as a guide to precise electrode placement. Lines of circumference were also inscribed to ensure that the six electrodes were placed in the same cross sectional plane.

Data was gathered at cross sectional positions beginning at two inches from the butt of each section. The electrode collar was moved in 2-inch increments from the initial position near the log-section butt until a position 2 inches from the top-end of the log section was reached. In each case twelve cross-sectional readings were obtained from each log.

For this experiment, electrode material was aluminum of less than 1 mm thickness and with a diameter of 1 inch. The electrodes were applied directly to log surface and held in place by the elastic electrode collar. Pairs of electrodes were then excited by attaching an alligator clip to the sending electrode. Likewise, an alligator clip was

attached to the appropriate receiving electrode. The voltage applied to the sending electrode was 112 volts at 500 KHz.

For an *n* electrode system, a combination of n readings will be obtained if only adjacent pairs are identified. Because the number of electrodes used were six, a total of six readings were taken at each cross-section position of the log. The six combinations of readings taken are listed in the Table 4.1 below.

Table 4.1

The six combinations of electrodes used to take the readings

Transmitting electrode	Receiving electrode
1	2
1	6
2	3
3	4
4	5
5	6

Following the acquisition of the total electrode combination data, the log-sections were crosscut at the circumferential positions corresponding to the electrode collar placement. The twelve resulting disks were $1^{15}/_{16}$ inches thick due to the removal of kerf at circumference lines. One face of each disk was photographed with a digital camera.

The photographed face was always oriented toward the butt section of the log. The first and last disk and the center disk of each log section were selected to determine wood moisture content and specific gravity. Moisture content was determined by the ASTM D4442-92 oven dry method [40] and specific gravity by the ASTM D2395-93 volumetric method [41].

Disks four inches away from knots on both sides were separated and were considered as clear disks. After separating the clear disks for each log section, the average voltage for each clear log section was calculated. This was achieved by calculating the mean of six electrode combinations shown in Table 4.1. Disks with knots were then selected and knot size, depth, and displacement with respect to the measuring electrode were measured.

The procedure that was employed to obtain knot depth, area, and displacement is illustrated in Figure 4.2 that shows a knot between electrodes one and six. A line was drawn from the periphery of the section through the center of the knot to the center of the disk using a ruler. Similarly, a line was drawn from the center point that each electrode would touch at the periphery of the section to the center of the log. If electrode one was considered as the transmitting electrode and electrode six as the receiving electrode, the angle made between the line through center of the knot with electrode one was considered as knot displacement. The distance from the edge of the disk to the top edge of the knot along the line connecting knot center and log center was considered as knot depth. Knot area was determined by measuring the radius of the knot. However, if the knot was an ellipse, its minor axis and major axes were measured and averaged.

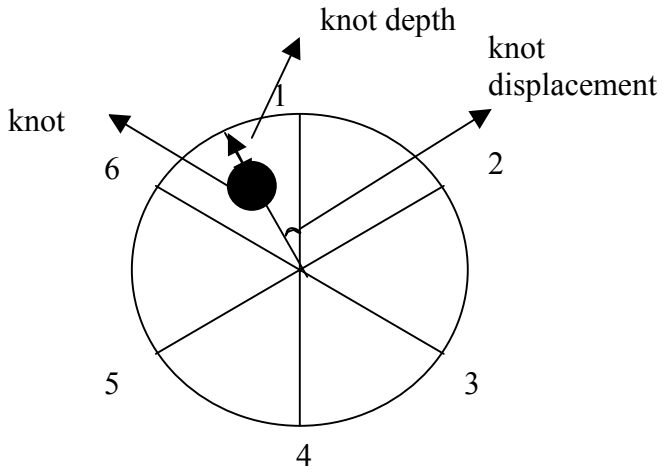

Figure 4.2: Measurement of knot depth, area and displacement.

CHAPTER V

SIMULATION MODEL CONSTRUCTION

5.1 Introduction

A finite element simulation of voltage response in the log sections was developed using ANSYS software. A 3-D electrostatic field analysis determined the output scalar potential caused by the applied input potential. The program was written in the form of a script with variables whose values can be changed to match physical conditions. The script variables are given in Table 5.1. All the variables were specified in terms of inches and volts.

Table 5.1

Parameters used in the ANSYS script

Parameter	Parameter name used in ANSYS
Wood diameter	od_
Sensor diameter	od2_
Wood relative permittivity	wdia_
Knot relative permittivity	ndia_
Length of the log.	extend1_, extend2_

The basic algorithm for modeling the voltage response requires the creation of a model of the log section with six electrodes attached around the log cross

section at every sixty-degree angle from the center of the log. Pairs of electrodes were then excited by applying load (voltage) to one electrode acting as a transmitter and response (voltage) was measured using a second electrode acting as a receiver. The following section describes the finite element procedure and issues employed with the script.

5.2 Simulation Model Procedure

The first step in the simulation design was to build the model, which involved defining the geometry, material properties, and element types [26,27,28]. In this script two types of elements were used. General elements used in three-dimensional electrostatic analysis are solid 122 and solid 123. Solid 122, which is a 3-D 20-node element, was selected to model the log under investigation since it is a well-suited element for curved boundaries [26]. A typical solid 122 element is shown in Figure 5.1. INFIN111, which is a 3-D infinite solid, was used to model the air surrounding the log. For an electrostatic field analysis, the permittivity material property should be defined [26]. Hence the permittivity property of INFIN111 was set to a constant value of one, while the permittivity property of solid 122 was used as an input variable whose value can be changed.

After defining the properties of the material, a finite element mesh of the model was generated by defining nodes and elements that describe the model geometry. There are two methods to generate a finite element model: solid modeling and direct generation. With solid modeling, the ANSYS program automatically meshes the geometry with nodes and elements. With direct generation, the user manually defines the location of

each node and the connectivity of each element. Due to the complexity involved in manually defining the location of each node in direct generation, solid modeling was used to generate the mesh. Because of the limitations of the software version, the size of each element in the mesh was set to 0.5. All these steps were performed using the commands available in the ANSYS preprocessor (PREP7). A typical three-dimensional model of the log section that is eight inches in diameter and ten inches long with six electrodes connected to it is shown in Figure 5.2.

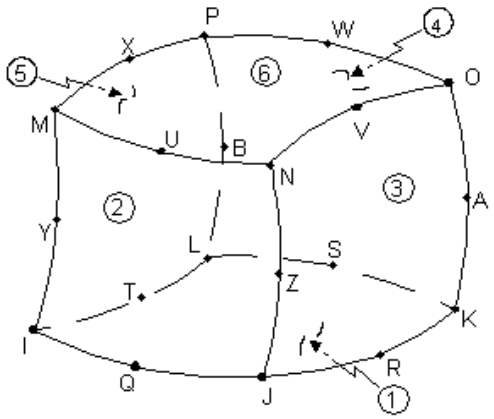

Figure 5.1: A typical Solid 122 element [26] .

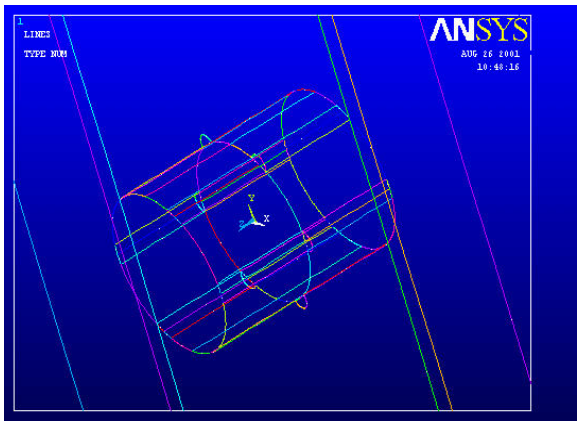

Figure 5.2: Three-dimensional model of a log with six electrodes attached to it.

Once the finite element model with desired material properties and element types was designed, the next step was to apply loads (voltage) and initiate the solution. Loads were applied using a set of commands available in the ANSYS postprocessor (POST1). Frontal solver, which is the default solver in ANSYS, was used to obtain the finite element solution.

At this point, the permittivity of the actual clear log sections was determined by simulating the log sections using the diameter data measured on actual log sections. The procedure used to determine the permittivity of clear log sections is described in chapter VI. Figure 5.3 shows a log that is 8 inches in diameter and 10 inches long, with electrode one excited with 112V.

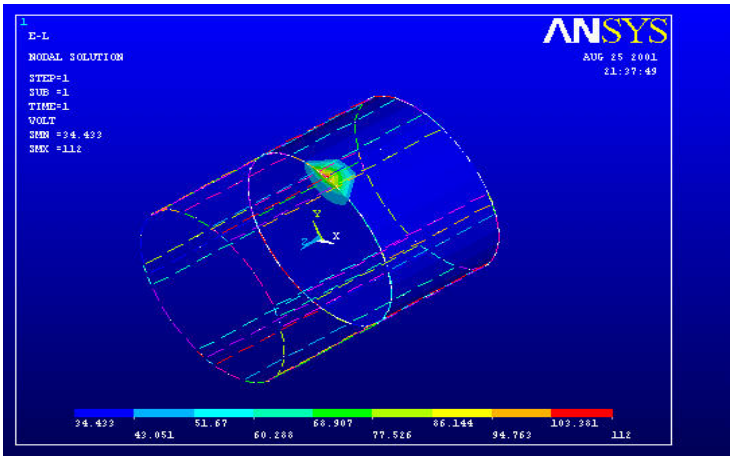

Figure 5.3: Three-dimensional model of a log with electrode one excited with 112 volts.

After obtaining clear wood permittivity values using the simulations, knots were added using the measurements made on actual log sections. The permittivity material property of the knots was used as an input variable whose value can be varied. The knot permittivity was determined using the procedure described in Chapter VI. Figure 5.4

shows a circular knot 2 inches in diameter, 0.5 inch deep that is located between electrodes one and two.

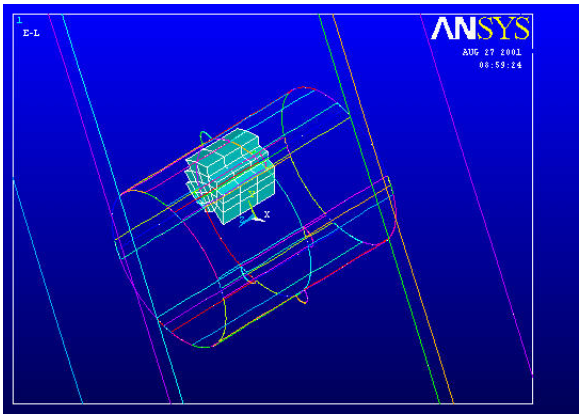

Figure 5.4: Three-dimensional model of a log with a knot of 2 inch in diameter and 0.5 inches depth.

CHAPTER VI

ANALYSIS, RESULTS AND DISCUSSION

6.1 Analysis Procedure

Clear wood procedure:

Clear wood permittivity values for each log section are determined using ANSYS software. This is achieved by estimating the resulting voltage values obtained by varying the permittivity from six to twenty four in increments of two for the six electrode combinations. For example, the simulated voltage values for different permittivity values for a particular log section is shown in Table 6.1. The permittivity value that yields the minimum difference between actual and simulated voltages is termed the *best permittivity* value for a particular log section. For the example in Table 6.1 the best permittivity value was 20, which provided the minimum difference between actual and simulated voltage results.

Model I is developed to determine the correlation between the moisture content, specific gravity, log diameter and actual clear wood voltage.

$$AV_{cw} = \beta_0 MC + \beta_1 SG + \beta_2 L_{dia} + error \qquad \text{Model I}$$

where: AV_{cw} = Actual voltage of clear wood

MC = Moisture Content (%)

SG = *Specific gravity*

L_{dia} = Diameter of the log

β_0 , β_1 , β_2 = Parameter estimates

Table 6.1

Actual and simulated clear wood voltage results for tested permittivity values. An asterisk in the difference column denotes the minimum actual to simulated difference and therefore the best permittivity value.

Electrode combination	clear wood permittivity								
	6	8	10	12	14	16	18	20	24
1 - 2	30.2	31.5	33.1	34.2	35.1	36.2	37.4	38.5	39.7
1 - 6	30.2	31.8	33.3	34.2	35.0	36.0	37.4	38.7	39.5
2 - 3	30.0	31.5	33.0	34.5	35.0	36.4	37.0	37.9	39.7
3 - 4	30.4	31.2	33.3	34.0	35.3	35.9	36.9	37.7	39.2
4 - 5	30.6	31.5	33.5	33.9	34.9	36.5	37.3	38.7	40
5 - 6	30.1	31.3	33.2	33.8	35.7	36.2	37.7	38.6	39.6
Simulated mean	30.25	31.47	33.2	34.1	35.17	36.2	37.28	38.35	39.6
Actual clear mean	38.7	38.7	38.7	38.7	38.7	38.7	38.7	38.7	38.7
Difference	8.45	7.23	5.5	4.6	3.53	2.5	1.42	.35 *	-0.9

Model II is developed to determine the correlation between the moisture content, specific gravity, log diameter and simulated clear wood voltage.

$$SV_{cw} = \beta_3 MC + \beta_4 SG + \beta_5 L_{dia} + error \qquad \text{Model II}$$

where:

SV_{cw} = Simulated voltage of clear wood

MC = Moisture Content (%)

SG = Specific gravity

L_{dia} = Diameter of the log

$\beta_3, \beta_4, \beta_5$ = Parameter estimates

Model III is developed to determine the correlation between the moisture content, specific gravity, log diameter and clear wood permittivity.

$$P_{cw} = \beta_6 MC + \beta_7 SG + \beta_8 L_{dia} + error \qquad \text{Model III}$$

where:

P_{cw} = Permittivity of clear wood

MC = Moisture Content (%)

SG = Specific gravity

L_{dia} = Diameter of the log

$\beta_6, \beta_7, \beta_8$ = Parameter estimates

Knot wood procedure:

After determining the optimal permittivity values for each clear log section; knots are simulated using the size, depth and displacement measurements made on actual knots. Voltage values for the six combinations are then estimated with permittivities of two, three and four using ANSYS software. Simulations are carried at permittivities of two, three and four because the difference between the simulated and the actual voltage is low

at these values. The voltage values for different knot permittivity values for a particular log section are tabulated as shown in Table 6.2.

Table 6.2

Voltage values for knot wood by permittivity value.

Electrode combination	Knot Wood Permittivity		
	2	3	4
1 – 2	25.2	26.3	27.0
1 – 6	27.2	26.7	28.1
2 – 3	35.7	37.9	37.9
3 – 4	37.7	37.7	37.7
4 – 5	37.7	37.75	37.75
5 – 6	38.0	38.2	38.2

Model IV is developed to determine the correlation between clear wood permittivity, knot area, knot depth, displacement and actual knot wood voltage. It is given by:

$$AV_{kw} = \beta_9 P_{cw} + \beta_{10} K_{area} + \beta_{11} K_{depth} + \beta_{12} K_{disp} + error \qquad \text{Model IV}$$

where:

AV_{kw} = Actual knot Voltage (volts)

P_{cw} = Permittivity of clear wood

K_{area} = Knot area (mm^2)

K_{depth} = Knot depth (mm)

K_{disp} = Knot displacement (%)

$\beta_9, \beta_{10}, \beta_{11}, \beta_{12}$ = Parameter estimates

Model V is developed to determine the correlation between clear wood permittivity, knot area, knot depth, displacement and simulated knot wood voltage. It is given by:

$$SV_{kw} = \beta_{13}P_{cw} + \beta_{14}K_{area} + \beta_{15}K_{depth} + \beta_{16}K_{disp} + error \qquad \text{Model V}$$

where:

SV_{kw} = Simulated knot Voltage (volts)

P_{cw} = Permittivity of clear wood

K_{area} = Knot area (mm^2)

K_{depth} = Knot depth (mm)

K_{disp} = Knot displacement (%)

$\beta_{13}, \beta_{14}, \beta_{15}, \beta_{16}$ = Parameter estimates

6.2 Results and Discussion

Linear regression analysis is performed using Model I, and the following equation is estimated. The corresponding P values are written below the equation.

$$AV_{cw} = 0.64MC + 138.1SG - 14.77L_{dia} \qquad \text{Model I estimated coefficients}$$

P_{values} (0.0001) (0.0001) (0.0001)

The Model I estimated coefficients show that the actual clear wood voltage decreased as the log section diameter is increased at an average rate of 14.77 volts per

inch. Similarly, the clear wood voltage increased as the moisture content is increased at an average rate of 0.64 volts per percent MC. Also, the clear wood voltage increased as specific gravity is increased at an average rate of 138.1 volts per gram per cubic centimeter. R^2 value, which represents the correlation between actual clear wood voltage and the model variables, is 0.92.

The Model II estimate coefficients show that the simulated clear wood voltage decreased as the diameter increased at an average rate of 14.73 volts per inch. Similarly, the clear wood voltage increased as the moisture content increased at an average rate of 0.63 volts per percent MC. Also, clear wood voltage increased as specific gravity increased at an average rate of 140.3 volts per gram per cubic centimeter. R^2 value, which represents the correlation between the simulated clear wood voltage and the model variables, is 0.95.

$$SV_{cw} = 0.63MC + 140.33SG - 14.73L_{dia}$$ Model II estimated coefficients

P_{values} (0.0001) (0.0001) (0.0001)

A comparison of Model I and Model II estimated coefficients show that the influence of all the three parameter estimates namely, log diameter, specific gravity and moisture content on actual and simulated voltages are nearly the same. R^2 value in the case of the simulated clear wood voltages is slightly higher than the actual clear wood voltages. The reason for this behavior may have resulted from experimental error in the data caused due to electrode placement and external noise.

Model III, which estimates the influence of log diameter, moisture content and specific gravity on simulated clear wood permittivity, show that the permittivity decreased as the diameter increased at an average rate of 9.55 units per inch as shown in

equation. Similarly, the permittivity increased as the moisture content and specific gravity increased at an average rate of 0.42 units per percent MC and 75.3 units per cubic centimeter. R^2 value for Model III is 0.91.

$$P_{cw} = 0.42MC + 75.3SG - 9.55L_{dia}$$ Model III estimated coefficients

P_{values} (0.0001) (0.0001) (0.0001)

The results using Model IV, which estimates the influence of the clear wood permittivity, knot area, knot depth, and knot displacement on the actual knot voltage, show that the clear wood permittivity, knot area, and knot depth significantly influenced the voltage response. The knot displacement, however, did not significantly influence the voltage response. Model IV estimates show that the actual knot wood voltage increased as clear wood permittivity increased at a rate of 0.727 units. Similarly knot wood voltage increased as the knot area, knot depth, and knot displacement increased at a rate of 0.004 units per mm^2, 0.0873 units per mm, and 0.028 units per degree respectively. R^2 value for Model IV is 0.92.

$$AV_{kw} = 0.72P_{cw} + 0.005K_{area} + 0.09K_{depth} + 0.03K_{disp}$$ Model IV estimated coefficients

P_{values} (0.0001) (0.0001) (0.0001) (0.168)

Model V estimated coefficients show that the influence of the clear wood permittivity, knot area, knot depth, and knot displacement on simulated knot wood voltage, significantly influenced the voltage response. However, the influence of knot displacement on knot voltage is slightly less than the remaining parameter estimates. Analysis of Model V yielded equation (6.4).

$$SV_{kw} = 1.542P_{cw} + 0.001K_{area} + 0.15K_{depth} + 0.08K_{disp}$$ Model V estimated coefficients

P_{value} (0.0001) (0.0001) (0.0001) (0.013)

Results using Model IV and Model V therefore indicate that it is possible to detect knot presence within the 60 degree angles of arc defined by pairs of adjacent electrodes using actual and simulated voltages. In addition, results for both actual and simulated voltages indicate the ability to estimate knot depth between electrode pairs. Knot location by displacement estimation was possible for simulated voltages but not for actual voltages.

The reason for knot displacement being insignificant for the actual voltage experiment might be because of the lack of sufficient data around the knots. Simulations showed that the effect of knots on voltage was high when the knot was near the exciting electrode. The effect of knots on the voltage was less or insignificant when the knots where at the receiving electrodes. Voltage values were recorded using the electrode combinations shown in Table 6.1. The current results indicate that voltage values should also be taken using the reverse combinations also. For example, electrode two should be excited and voltage should be measured at electrode one. Therefore, estimation of angular knot position between electrode pairs may be possible with improved data gathering procedure.

A more detailed comparison of the simulated versus actual voltage required eliminating knot displacement because it did not significantly influence actual voltage. For this purpose Models IV and V were rewritten as Models VI and VII respectively.

$$AV_{kw} = \beta_{17} P_{cw} + \beta_{18} K_{area} + \beta_{19} K_{depth} + error \qquad \text{Model VI}$$

$$SV_{kw} = \beta_{20} P_{cw} + \beta_{21} K_{area} + \beta_{22} K_{depth} + error \qquad \text{Model VII}$$

Analysis of Model VI and Model VII yielded the following estimated coefficients.

$$AV_{kw} = 0.764P_{cw} + 0.005K_{area} + 0.093K_{depth}$$ Model VI estimated coefficients

P_{values} (0.0001) (0.0001) (0.0001)

$$SV_{kw} = 1.645P_{cw} + 0.004K_{area} + 0.123K_{depth}$$ Model VII estimated coefficients

P_{values} (0.0001) (0.0001) (0.0001)

R^2 results for the estimated coefficients of Model VI and VII were 0.92 and 0.98 respectively showing good fit to both simulated and actual data.

While coefficient results obtained from both Model VI and Model VII differed slightly both indicate that the knot wood voltage increased as the clear wood permittivity, knot area, and knot depth increased. Increase in knot wood voltage values as the knot depth increased signifies that the effect of knots on voltage decreased as the knot depth increased.

CHAPTER VII

SUMMARY

A script is developed using ANSYS finite element software to model defect detection of knots in logs. Initially, experimental data is collected on actual log sections that contained knots and clear wood. Then the permittivity of clear wood for each log section is determined using the simulation procedure. Knots are then added into the simulated log sections using the measurements made on actual data. It is observed that the presence of knots affected the voltage values between pairs of electrodes.

Both simulated and actual clear wood voltages between adjacent electrodes were influenced similarly. The voltage decreased at a rate of 14.7 volts per inch of log section diameter increase. Specific gravity increased at about 140 volts for each one-unit gcm^3 increase. Voltage increased at about 0.6 volts per percent increase in moisture content.

Best simulated permittivity to provide the actual clear wood voltages observed were determined for each log section. Best permittivity values varied considerably and ranged from 10 to 20. However, the best permittivity variance was well explained by the significant influence of wood moisture content, specific gravity and log section diameter. R^2 value for this relationship was 0.91.

The influence of clear wood permittivity, knot area, knot depth, and knot displacement on both simulated and knot wood voltages was determined. Voltage

increased as the permittivity, knot area, and knot depth increased. The knot displacement did not show much influence on the actual knot voltages. R^2 values were 0.92 and 0.98 for actual and simulated knot wood voltages. Results indicated that is possible to detect knot presence with the 60-degree angles of arc defined by pairs of adjacent electrodes.

7.1 Future Work

The modeling of knots in the log sections is an area that requires further improvement. Though simulation of knots is accurate, compression wood, which is located around the knots, is not taken into consideration. Compression wood might contain different properties than clear and knot wood due to which the voltage response might vary.

To perform the simulations with better speed and considerable accuracy, the simulations are performed with an assumption of a rectangular ground box with its sides located equidistant around the log. But in the real environment, the ground is very near compared to the walls of the room. To make the simulation look more similar to the real conditions, the left, right, and top sides of the box should be much farther compared to the bottom of the box. Using a very high speed computer, simulations can be more accurately performed with actual boundaries.

Due to the limitations of the software version, the least possible size of the element that is possible is 0.5. The mesh is very coarse and the circular knot added to the log section did not show up to be circular. Upgrading the software version might improve the model.

The measurements are performed with the concrete floor acting as a ground. Measurement accuracy can be improved by using a conducting material to define the ground plane.

Voltage values are taken using adjacent pairs of electrodes. Due to this reason, knots that are in the center of the log did not affect the adjacent voltage readings. Hence voltages should be measured using different combinations of electrodes. Results proved that knot displacement did not show any influence on the voltage. Simulations showed that measurement of voltages in the reverse direction improves the knot defect detection. Hence measurement of voltages on the actual logs in the reverse order might improve the influence of knot displacement.

REFERENCES

[1] Tsolakides, J. A. "A simulation model for log yield study," *Forest Prod. J.* 19(7): 21-26.1969.

[2] Wagner, F. G. and F. W. Taylor, "Simulated sawing with a chipping headrig," *Forest Prod. J.* 25(10): 24-28. 1975.

[3] Richards, D. B., W. K. Adkins, H. Hallock, and E. H Bulgrin, "Lumbe Values from computerized simulation of hardwood log sawing," Res. Pap. FPL-356. USDA Forest Serv., Forest Prod. Lab. 28 pp., 1980.

[4] Peter, R. K. "Lumber grade yield from yellow-polar," *Forest Prod. J.* 17(11): 19-24, 1967.

[5] J. W. S. Hearle, "The Relation between Structure, Dielectric constant and Electrical Resistance of Fibers," *Jour. Textile Institute Transaction*, 48:40, 1957.

[6] Schmoldt, D. L., Zhu, D, and Conners, R. W. "Nondestructive evaluation of hardwood logs using automated interpretation of CT images," in Review of Progress in Quantitative Nondestructive Evaluation, ed. By Thompson, D.O. and Chimenti, D.E. Vol. 12,Plenum Press, New York p.2257-2264, 1993.

[7] D. Zhu, A. Beex, "Robust spatial auto-regressive modeling for hardwood log inspection," *Journal of visual communication and image representation*, Vol. 5, No. 1, March, pp. 41-51,1994.

[8] P. A. Araman, D.L. Schmoldt, "Scanning system, technology worth a look," *Wood and wood products*, 1995(April).

[9] Anders Kaestner, "Polarimetry Based Wood Scanning. Theory and Experiments," Thesis for the degree LICENTIATE OF ENGINEERING, Nov 1999.

[10] Davis, J. R., "Internal scanning of wood using computerized tomograpy," 1986 Gottstein Report 64pp. The Joseph William Gottstein Memorial Trust Fund, Victoria, Australia, 1986.

[11] Chang, S. J. "External and internal defect detection to optimize cutting of hardwood logs and lumber". A report prepared for the technology transfer information center, National Agricultural Library, US Department of Agriculture, and the National Institute of Standards and Technology, US Department of commerce, under contract agreement 58-0520-1-157 with the University of Maine, 1992.

[12] J. Aune, "An X-ray log-scanner for sawmills," in *2nd international seminar/workshop on scanning technology and image processing on wood*, pp. 51-64, 1995.

[13] Hagman, "Automatic grading of logs with TINA, a gamma ray log scanner," in *proceedings from the seminar/workshop on scanning technology and image processing on wood*, 1992.

[14] Brian V. Funt, Edwin C. Bryant, "Detection of internal log defects by automatic interpretation of computer tomography images," *Forest product Journal.* 37(1): 56-62, 1987.

[15] Sindre Holoyen and Rolf Birkeland, "Industrial Methods for Internal Scanning of Log Defects," *A Progress Report on an Ongoing Project in Norway. Scanning Technology and Process Optimization. Miller publications*. Pg.: 61-73, 1999.

[16] Schmoldt, D. L., Li, P. and Abbott, A. L, "CT Imaging of hardwood logs for lumber production" in Askin, R.G., Bidanda, B. and Jagdale, S. (ed) *Proceedings of 5th Industrial Engineering Research Conference*, May 18-20,1996,Minneapolis, Minnesota, USA p.387-392, 1996b.

[17] Chang, S. J., J. R. Olson, and P. C. Wang, "NMR imaging of internal features in wood," *Forest Products Journal* 39(6): 43-49,1989.

[18] Schafer, Mark, E. "Ultrasonic apparatus for characterizing wooden members using a measurement of wave distortion," International publication Number: WO 99/44049.,1999.

[19] David W. Prine, "Microwave flaw detection system having horns positioned with their polarization directions transverse to each other," U.S. Patent 3,549,986, Dec. 22, 1970.

[20] Kinanen, et al., "Method for classifying and measuring of timbers," U.S. Patent 4,123,702, October 31, 1978.

[21] Heikkila; Sakari, "Method and apparatus for detecting grain direction in wood, particularly in lumber," U.S. Patent 4,500,835, February 19, 1985.

[22] Bechtel, et al., "Apparatus and method for measuring wood grain angle," U.S. Patent 4,972,154, November 20, 1990.

[23] Steele Philip. H, Kumar Lalit, "Detector for heterogeneous materials," U.S. Patent 5,585,732, December 17, 1996.

[24] Svenson , et al., "Electromagnetic imaging and therapeutic (EMIT) systems," U.S. Patent 6,026,173, February 15, 2000.

[25] Beck, et al., "Tomographic flow imaging system," U.S. Patent 5,130,661, July 14, 1992.

[26] Ansys 5.6 help system.

[27] David S. Burnett, "Finite element analysis from concepts to applications" Addison-Wesley publishing company. ISBN 0-201-10806-2.

[28] Matthew N. O. Sadiku, "Elements of electromagnetics," Second edition. Oxford University press. ISBN 0-19-510368-8.

[29] Hirai, S. and K. Kitahara, *Wood Physics*. Asakura Book Corp. Tokyo, Japan. P. 39-41, 1953.

[30] Skaar, "The dielectric properties of wood at several radio frequencies," N.Y. state Coll. Of forest Tech. Pub. No. 69.,1948.

[31] Uyemura, T. "Dielectric properties of wood as the indicator of the moisture," Bull Gov. For. Exp. Sta. No. 119, 95-172, Tokyo, Japan,1960.

[32] J. J. Wittkoff and M.D. Macdonald, "Dielectric properties of Douglas Fir at high frequencies," Oregon State College, Bulletin No. 28, 1949.

[33] William L. James, "Dielectric properties of wood and hardwood: variation with temperature, frequency, moisture content and grain orientation," USDA forest service Research paper FPL 245, 1975.

[34] Siau, J. F. "Wood: Influence of moisture on physical properties", Department of wood science and forest products, Virginia Polytechnique Institute and State University. Blacksburg, VA.

[35] R. T. Lin, "Review of the dielectric properties of wood and cellulose," Oregon State University, Corvallis, Oreg.,1969.

[36] R. W. Skaar, "Mechanism of electrical conduction in wood," *Forest products journal*. 13(10): 455-459, 1963.

[37] A. Venkateswaran and Shiva Yogi Tiwari, "Dielectric properties of moist wood," TAPPI 47(1) 25-28, 1964.

[38] A. Venkateswaran, "A note on Densities and conductivities of wood," *Wood Science* vol. *5,* No. 1, July 1972.

[39] Stamm, A. J, *Wood and Cellulose Science*. Ronald Press, N.Y. p.367, 1964.

[40] American Society for Testing Materials. "Standard test methods for specific gravity of wood and wood-based materials," ASTM D2395-93. ASTM. Philadelphia, PA. pp. 348-355, 1996.

[41] American Society for Testing Materials. "Standard test methods for direct moisture content measurements of wood and wood-based materials," ASTM D4442-92. ASTM. Philadelphia, PA. pp. 348-355, 1996.

APPENDIX A

ANSYS SOFTWARE

Running Ansys Software:

Goto: programs>Ansys 5.7 > Interactive

Then in the GUI that pops up, select the working directory. Then hit the "RUN" botton.

After you hit Run button, five GUIs will pop up. In the Utility menu, you have file option, where you can read the file, save the file, etc. It is better if the program is written in the form of a script. The extension of the file in which the script is written should be saved as a ".mac" extension (ex: "input.mac").

Simulating a log with clear wood only:

Lets say you have a code for simulating a log with clear wood in the file input8.mac that is at C:\temp\ansys\tutorial. In order to run the file follow the steps below.

Step 1: Change the parameters that are specified in the clear log section file that matches the actual log section.

Step 2: In the Interactive GUI that pops up when ansys is started, specify the path in the working directory option.

Step 3: From the Utility menu that pops up, goto file>read input from. Then select the file input8.mac. The software will perform the simulations for the clear wood.

Simulating a log with knot wood:

Prior to simulating the knots, we **must** simulate the clear wood log section. To simulate knot wood you need to have the information regarding the size, depth and displacement of the knot. Knot wood code can be written in the same file as clear log file or it can be written in a different file.

To add a circular knot after simulating the clear wood use the following code. The code below adds a circular knot that has a permittivity of 2. The center of the knot makes an angle of 60 degree with electrode 2. The center of the knot is at a distance of 2.9 inches from the center of the log and is 0.6 inches in radius.

```
/prep7
ndia_= 2                    !knot relative permitivity
MP,PERX,3,ndia_      !relative permitivity knot
wpcsys,-1,0       !defines the working plane location based on a coordinate system
wprot,60,,        !Rotate the working plane to 60 degree.
wpoff,2.9,0,0     !move the working plane to centre of knot position.
CSWPLA,11,1,1,1,  !circular coordinate system.
csys,11
```

```
x1=0            ! specify the x,y,z values of knot.
x2=0.6
y1=0
y2=360
z1=0
z2=0.6
nsel,s,loc,x,x1,x2        !x1 and x2 are spatial coords
nsel,r,loc,y,y1,y2        !y1 and y2 are spatial coords
nsel,r,loc,z,z1,z2        !z1 and z2 are spatial coords
esln
nsel,all
esel,r,mat,,1
!then run this command:
emodif,all,mat,3          !change the added knot material property to 3.
```

A second knot can be added using the same code as above.

Changing simulation variables:

Simulation variables can be changed in the file. Once you change the variables, you need to save it and run it again using the steps shown in simulating a log with clear wood only.

Save/ Retrieve simulation results:

Generally results are displayed on the dos command window. If you want to save the simulation, it should be saved as ".db" extension. You have save as option in the file option. To retrieve the simulation use "resume from" option that is listed in file option. Then goto plot>multi-plots in the utility menu to get the complete image.

Saving and image as a jpg file:

In order to save the image using the following steps:

Step 1: Goto Plotctrls>hard copy>To file.

Step 2: select an option. (i.e. jpep or bmp etc).

Step 3: then in the save to option, specify the file name and press ok.

Ansys online help tutorial:

The best way to learn Ansys is to use the online help tutorial. It has some good examples in different applications. Step by step procedure is given in the tutorial. Also if you need any information regarding a command, ansys index can be used. In order to use ansys

help tutorial goto Help option in Ansys utility menu. If you want any information regarding any ansys command, click on “help topics”. If you want to go through the tutorial click on “Ansys tutorials”.